LA-UR-13-29555 (Accepted Manuscript)

Influence of heterogeneity on second-kind self-similar solutions for viscous gravity currents

Zheng, Zhong
Christov, Ivan
Stone, Howard A

To be published in: Journal of Fluid Mechanics

DOI to publisher's version: 10.1017/jfm.2014.148

Permalink to record: http://permalink.lanl.gov/object/view?what=info:lanl-repo/lareport/LA-UR-13-29555

Influence of heterogeneity on second-kind self-similar solutions for viscous gravity currents

Zhong Zheng[1], Ivan C. Christov[1,2], and Howard A. Stone[1]†

[1]Department of Mechanical and Aerospace Engineering,
Princeton University, Princeton, New Jersey 08544, USA

[2]Theoretical Division and Center for Nonlinear Studies,
Los Alamos National Laboratory, Los Alamos, New Mexico 87545, USA

(Received ?; revised ?; accepted ?. - To be entered by editorial office)

We report experimental, theoretical and numerical results on the effects of horizontal heterogeneities on the propagation of viscous gravity currents. We use two geometries to highlight these effects: (*a*) a horizontal channel (or crack) whose gap thickness varies as a power-law function of the streamwise coordinate; (*b*) a heterogeneous porous medium whose permeability and porosity have power-law variations. We demonstrate that two types of self-similar behaviors emerge as a result of horizontal heterogeneity: (*a*) a first-kind self-similar solution is found using dimensional analysis (scaling) for viscous gravity currents that propagate away from the origin (a point of zero permeability); (*b*) a second-kind self-similar solution is found using a phase-plane analysis for viscous gravity currents that propagate toward the origin. These theoretical predictions, obtained using the ideas of self-similar intermediate asymptotics, are compared to experimental results and numerical solutions of the governing partial differential equation developed under the lubrication approximation. All three results are found to be in good agreement.

Key words: Gravity currents, Hele-Shaw flows, Porous media

1. Introduction

The gravitationally driven spreading of viscous fluids, also known as viscous gravity currents, is a process common to a large number of industrial and geological phenomena (Hoult 1972; Simpson 1982; Huppert 2000, 2006). One aspect of their propagation has been particularly attractive, namely the ability, after a sufficient amount of time has elapsed, to obtain the spatial distribution, or shape, of the current at different times through a transformation of the independent variables. In other words, once the initial condition is "forgotten", gravity currents evolve in a *self-similar* fashion (Sedov 1993; Barenblatt 1996). As a result, the self-similar propagation of gravity currents, which can be understood as intermediate asymptotics in the sense of Barenblatt & Zel'dovich (1972), has been studied in detail; see, e.g., the mathematical framework for problems of this type discussed by Gratton & Minotti (1990) and the references therein.

One-dimensional gravity currents in homogeneous porous media have been of particular interest (see, e.g., Huppert 2006). In unconfined porous media, self-similar solutions of the first kind—whose scaling exponents can be determined by simple balances of terms

† Email address for correspondence: hastone@princeton.edu

in the governing equations—were obtained by Barenblatt (1952) and Pattle (1959) to describe the spread of a finite mass of fluid. The latter solutions were extended to apply to propagation due to fluid injection and shown to agree with laboratory experiments in both Hele-Shaw cells (see, e.g., Huppert & Woods 1995) and systems of packed beads (see, e.g., Lyle *et al.* 2005). In soil mechanics, the propagation of a gravity current into an unsaturated soil is known as infiltration (Philip 1970; Bear 1972), and self-similar solutions of the first kind have also been adapted as approximations for infiltration into homogeneous layers with a pre-existing moisture distribution (Witelski 1998). A wealth of first-kind self-similar solutions also describe the early and late time propagation regimes through a homogeneous porous medium lying above an inclined impermeable boundary (see, e.g., Vella & Huppert 2006), over fractured horizontal substrates (see, e.g., Pritchard 2007) and for drainage from the edge of a finite porous reservoir (Zheng *et al.* 2013). In confined porous media, on the other hand, a rarefaction wave self-similar solution was derived, and verified by numerical simulations, to describe the evolution of the immiscible interface between a fluid being injected at a constant rate and the more viscous fluid being displaced (Nordbotten & Celia 2006); seepage through the confining layer has also been considered (Woods & Farcas 2009). Further work revealed that, after injection ceases, there is a transition from an early time self-similar behavior to a late time self-similar behavior, and again the theoretical results were supported by numerical simulations (Hesse *et al.* 2007). Direct numerical simulations have shown that the presence of transverse sidewalls can affect the selection of a self-similar propagation regime or the transition from one to the next (Hallez & Magnaudet 2009).

Two-dimensional and axisymmetric propagation of viscous gravity currents has also been studied, given the possible practical applications to fluid injection into wells and subsurface reservoirs. For a viscous current propagating away from the center of a horizontal plate, a first-kind self-similar solution was found in an unconfined system and in a porous medium (Barenblatt 1952; Pattle 1959; Kochina *et al.* 1983), verified experimentally for spreading into an inviscid fluid (e.g., air) (Didden & Maxworthy 1982; Huppert 1982), and in a system of packed beads (see, e.g., Lyle *et al.* 2005). The axisymmetric propagation of a power-law non-Newtonian gravity current into an inviscid fluid (e.g., air) has also been studied (Gratton *et al.* 1999). For non-axisymmetric configurations, gravity currents in unconfined systems arising from both point and line sources (Lister 1992), converging flows (Diez *et al.* 1998) and currents in porous media (Vella & Huppert 2006; De Loubens & Ramakrishnan 2011) have been considered.

An interesting feature of the axisymmetric problem is that self-similar solutions of the *second kind* exist for the case of propagation toward the center of a horizontal plate (Gratton & Minotti 1990; Angenent & Aronson 1995), and these were found to agree with experiments (Diez *et al.* 1992). Second-kind self-similar solutions, unlike those of the first kind, cannot be obtained by a scaling analysis of the governing partial differential equation (PDE) (Barenblatt & Zel'dovich 1972; Barenblatt 1996; Eggers & Fontelos 2009) but rather are constructed by a more involved mathematical analysis. The significance of this step is that there are propagation modes for viscous gravity currents that can only be obtained via a phase plane analysis (Sedov 1993; Courant & Friedrichs 1999) of the governing PDE, which requires the numerical solution of a nonlinear eigenvalue problem for the scaling exponent in the similarity variable (Barenblatt & Zel'dovich 1972; Barenblatt 1996).

Heterogeneity always exists in real-world porous media, and it may significantly affect the propagation regimes of viscous gravity currents. When there exists a power-law permeability gradient in the vertical direction, the propagation and drainage processes in a porous medium are modified from the homogeneous case (Huppert & Woods 1995;

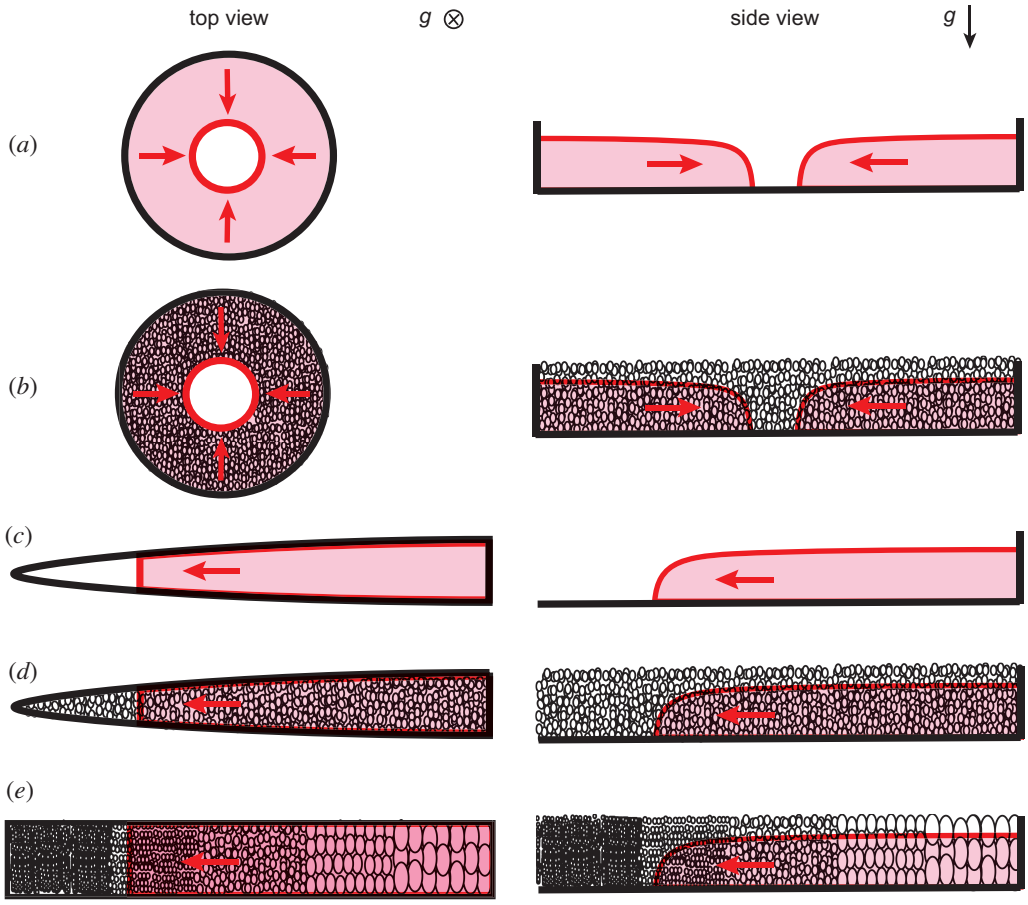

FIGURE 1. Different flows of viscous gravity currents, propagating toward a coordinate system's origin, that may be described by self-similar solutions of the second kind. (*a*) Converging viscous gravity currents on a horizontal substrate (Gratton & Minotti 1990; Diez *et al.* 1992; Angenent & Aronson 1995); (*b*) converging currents in homogeneous porous media; (*c*) viscous gravity currents propagating in horizontal channels with varying gap thickness of power-law form; (*d*) currents propagating horizontally in homogeneous porous media with converging boundaries of power-law form; (*e*) currents propagating in heterogeneous porous media with permeability and porosity gradients in the horizontal direction.

Takagi & Huppert 2007; Zheng *et al.* 2013; Ciriello *et al.* 2013). In vertically layered systems with permeability jumps across layers, flow focusing can occur and may even dominate over buoyancy as the key physical transport mechanism (Huppert *et al.* 2013). In general, homogenization techniques must be employed in such cases to derive a depth-averaged governing equation for the current (Anderson *et al.* 2003). It should be noted that heterogeneity exists not only in the vertical but also in the horizontal direction in real-world systems. For example, porous media may have horizontal permeability and porosity gradients on the reservoir scale (Bear 1972; Class *et al.* 2009), while individual channels and cracks in the porous medium can have varying gap thickness in the streamwise flow direction (Spence & Sharp 1985; Detournay 2004). To the best of our knowledge, the propagation of viscous gravity currents into media with horizontal heterogeneity has only been studied previously by Ciriello *et al.* (2013), however, they only

considered first-kind self-similar solutions and assumed the porosity of the medium to be constant.

The goal of this paper is to study the effects of horizontal heterogeneity on the propagation of viscous gravity currents. As we document below, horizontal heterogeneity allows for both first- and second-kind self-similar currents. Figure 1 shows a summary of the physical situations in which we expect self-similarity of the second kind: (a) converging currents on a horizontal substrate (Gratton & Minotti 1990; Diez *et al.* 1992; Angenent & Aronson 1995); (b) converging currents in an unconfined homogeneous porous medium; (c) currents propagating in horizontal channels or cracks with varying gap thickness of power-law form; (d) currents propagating in a homogeneous porous medium with converging boundaries of power-law shape in the horizontal direction; and (e) currents propagating in heterogeneous porous media with power-law permeability and porosity gradients in the horizontal direction.

In this work, we analyze in detail the effects of heterogeneity, specifically case (c) is studied in §2.1 and case (e) is studied in §2.2. In addition, we briefly discuss cases (b) and (d) in Appendices A.1 and A.2, respectively. We show that viscous gravity currents propagating away from the origin (a point of zero permeability) are described by first-kind self-similar solutions, while currents propagating toward the origin are described by second-kind self-similar solutions. A novel conservative implicit finite-difference scheme is developed (Appendix B) to numerically solve the governing partial differential equation. In §3, the results from analyses based on self-similar intermediate asymptotics are shown to agree well with the numerical solutions and laboratory experiments.

2. Formulation of the mathematical model

2.1. *Gravity currents in channels*

Hele-Shaw cells, i.e., channels created by two closely spaced plates are an ideal system in which to study the propagation of viscous gravity currents spreading into an inviscid fluid (e.g., air) or into a porous medium. To formulate a mathematical model of these processes, we assume that the invading and displacing fluids are immiscible, separated by a sharp interface, and we only consider the limit of negligible surface tension. Additionally, in the present work, the invading fluid always has greater viscosity than the displaced fluid, so that the interface is not susceptible to the Saffman–Taylor viscous fingering instability (Saffman & Taylor 1958; Homsy 1987). The viscous gravity current in the channel is long and thin, so the lubrication approximation applies, and the flow is horizontal to leading order in the aspect ratio; velocity components in the vertical and cross-stream direction are neglected. Given the unconfined nature of this flow problem, in the following, we also assume motion of the displaced fluid is negligible since the upper layer is sufficiently deep.

2.1.1. *Flow away from the origin*

Consider a viscous gravity current propagating in a horizontal channel in the direction of increasing gap thickness, away from the origin of the chosen coordinate system (see figure 2(a)). We denote by $h(x,t)$ the shape of the current and by $x_f(t)$ the location of the moving front (nose of the current) such that $h(x_f(t),t) = 0$. We assume that the gap thickness of the channel has a power-law form: $b(x) = b_1 x^n$, where b_1 and n are non-negative real numbers.

The lubrication approximation holds, if $|db/dx| \ll 1$ and $|\partial h/\partial x| \ll 1$, except perhaps at the nose of the current. However, note that for the assumed shape $b(x)$ and $n > 1$, the requirement that $|db/dx| \ll 1$ is violated when the nose of the current $x_f \approx (nb_1)^{1/(1-n)}$.

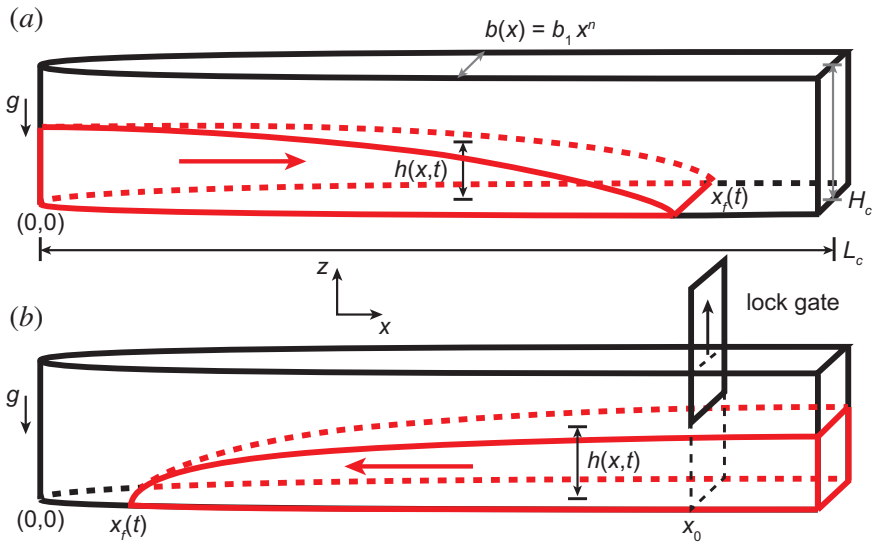

FIGURE 2. Diagram of the geometry of a horizontal channel with varying gap thickness $b(x)$ in which a viscous gravity current is propagating. The shape of the current and the position of the front are denoted by $h(x,t)$ and $x_f(t)$, respectively. (a) Propagation away from the origin in the direction of increasing gap thickness. (b) Propagation toward the origin, from far downstream, in the direction of decreasing gap thickness. Gravity is directed in the negative vertical (i.e., $-z$) direction.

Also, the lubrication approximation fails when the aspect ratio $b(x_f)/x_f \approx 1$ (for propagation away from the origin), or $x_f \approx b_1^{1/(1-n)}$; specifically, the cross-stream velocity is no longer negligible, and the propagation of the gravity current is not described by a one-dimensional model. Moreover, we see that for $n > 1$, $b(x)/x$ is an increasing function of x, hence there is a maximal propagation distance, $x_f = O\left(b_1^{1/(1-n)}\right)$, beyond which the one-dimensional lubrication model fails. Meanwhile, for $n < 1$, $b(x)/x$ is a decreasing function of x, hence $b(x) < x$ holds for all $x > O\left(b_1^{1/(1-n)}\right)$; although $b(x_f)/x_f \approx 1$ near the origin for $n < 1$, this in an initial, localized effect that does not affect the overall applicability of the lubrication approximation for the gravity current's propagation.

Under the above assumptions, Darcy's law in the horizontal direction and the one-dimensional form of the continuity equation, respectively, take the form

$$u = -\frac{k(x)}{\mu}\frac{\partial p}{\partial x}, \tag{2.1a}$$

$$\frac{\partial}{\partial t}(hb) + \frac{\partial}{\partial x}(hub) = 0, \tag{2.1b}$$

where u is the transversely averaged horizontal velocity, k is the effective permeability of the medium, p is the fluid pressure, and μ is the viscosity of the invading fluid. In the vertical direction, the pressure field is hydrostatic: $p(x,z,t) = p_0 + \Delta\rho g\big(h(x,t) - z\big)$, where p_0 is the ambient pressure in the displaced fluid and $\Delta\rho$ is the density difference between the two fluids (Huppert & Woods 1995).

Following standard steps (Barenblatt 1996; Huppert & Woods 1995), we substitute the hydrostatic pressure distribution and the gap thickness $b(x) = b_1 x^n$ into equation (2.1); we neglect drag on the bottom plate and assume h is sufficiently greater than b so that the permeability is given by $k(x) = b(x)^2/12$. Then, we obtain a nonlinear diffusion

equation for the current height:

$$\frac{\partial h}{\partial t} - \frac{A}{x^n}\frac{\partial}{\partial x}\left(x^{3n} h \frac{\partial h}{\partial x}\right) = 0, \tag{2.2}$$

where $A = (\Delta \rho g b_1^2)/(12\mu)$. The case of a channel with constant gap thickness is recovered by setting $n = 0$.

To maintain generality, we define the injection rate as $\gamma Q t^{\gamma-1}$ so that, at any time, the total volume of injected liquid is Qt^γ, where $\gamma \geqslant 0$. Since the gravity current is moving away from the origin $x = 0$, the global mass conservation constraint has the form

$$\int_0^{x_f(t)} x^n h(x,t)\,\mathrm{d}x = Bt^\gamma, \tag{2.3}$$

where $B = Q/b_1$. We expect that the details of the solution will depend on n and γ.

From a scaling analysis of equations (2.2) and (2.3), we find that the appropriate similarity variable is

$$\xi = \frac{x}{(AB)^{1/(3-n)} t^{(\gamma+1)/(3-n)}}, \tag{2.4}$$

from which it immediately follows that front of the current moves according to

$$x_f(t) = \xi_f(n,\gamma)(AB)^{\frac{1}{3-n}} t^{\frac{\gamma+1}{3-n}}, \tag{2.5}$$

where the pre-factor $\xi_f(n,\gamma)$ is a constant that depends only on the values of n and γ. We define $y \equiv x/x_f(t) = \xi(x,t)/\xi_f(n,\gamma)$, after which the shape of the current can be written as

$$h(x,t) = \xi_f^{2(1-n)} A^{\frac{n+1}{n-3}} B^{\frac{2(n-1)}{n-3}} t^{\frac{2(n-1)\gamma+(n+1)}{n-3}} f(y), \tag{2.6}$$

where $f(y)$ and $\xi_f(n,\gamma)$ are solutions to the following system:

$$(y^{3n} f f')' - \left(\frac{\gamma+1}{n-3}\right) y^{n+1} f' - \left(\frac{2(n-1)\gamma+(n+1)}{n-3}\right) y^n f = 0, \tag{2.7a}$$

$$f(1) = 0, \tag{2.7b}$$

$$\xi_f(n,\gamma) = \left(\int_0^1 y^n f(y)\,\mathrm{d}y\right)^{1/(n-3)}, \tag{2.7c}$$

and primes denote differentiation with respect to y. For $n = 0$, equation (2.7) reduces to the homogeneous porous medium case in Cartesian coordinates (Huppert & Woods 1995). In this class of problems, one boundary condition is sufficient to uniquely determine the solution, owing to the form of the singularity at the front.

Following Huppert (1982), we can determine the asymptotic behavior of the current near the nose from (2.7*a*,*b*):

$$f(y) \sim \left(\frac{\gamma+1}{3-n}\right)(1-y) \quad \text{as} \quad y \to 1^-, \tag{2.8}$$

which can, in turn, be used to provide two boundary conditions near $y = 1$, i.e., $f(1-\nu)$ and $f'(1-\nu)$, $\nu \ll 1$, in a shooting procedure for solving equation (2.7*a*) numerically. Typical numerically computed current shapes $f(y)$ are shown in figure 3 for (*a*) constant volume ($\gamma = 0$) and (*b*) constant injection rate ($\gamma = 1$) and various choices of n. The dependence of ξ_f on γ is illustrated in figure 3(*c*) for various choices of n.

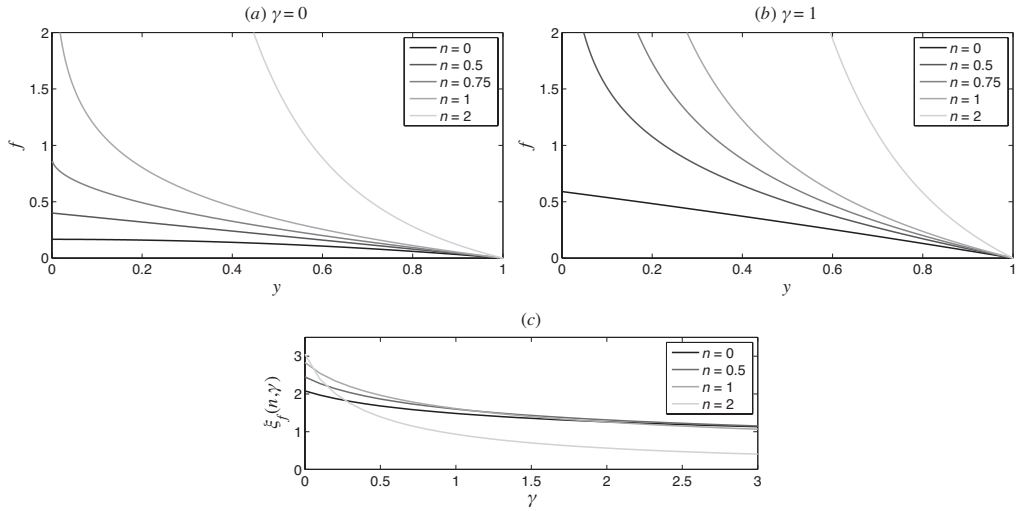

FIGURE 3. Self-similar shape of a viscous gravity current propagating away from the origin in a channel with variable gap thickness of the form $b(x) = b_1 x^n$ for (a) constant volume ($\gamma = 0$) and (b) constant injection rate ($\gamma = 1$), and various values of n; the pre-factor $\xi_f(n, \gamma)$ is shown in panel (c). The solutions for f were found by integrating equation (2.7a) numerically by shooting backwards from $y = 1 - \nu$ ($\nu = 10^{-4}$), where boundary conditions on f and f' are imposed using the asymptotic form from equation (2.8).

For $\gamma = 0$ and $0 \leqslant n < 3$, equation (2.7) has the exact solution

$$f(y) = \begin{cases} \dfrac{1}{2(n-1)(n-3)} \left(1 - y^{2(1-n)}\right), & n \neq 1, \\ -\frac{1}{2} \ln y, & n = 1, \end{cases} \tag{2.9a}$$

$$\xi_f(n, 0) = \left[(n+1)(n-3)^2\right]^{1/(3-n)}. \tag{2.9b}$$

For $n = 0$, this solution reduces to a special case of the Barenblatt–Pattle point-source solution (Barenblatt 1952; Pattle 1959). For $n \geqslant 3$, the self-similar solution represents a receding front because $(\gamma + 1)/(3 - n) < 0$, which has also been observed in higher-order lubrication models (King & Bowen 2001; Flitton & King 2004). However, in the present case, the first-kind self-similar solution for $n \geqslant 3$ is unphysical because $f < 0$, which means the height of the current is negative.

2.1.2. *Flow toward the origin*

In this section, we consider the opposite case of a viscous gravity current propagating in the direction of decreasing gap thickness, i.e., toward the origin (see figure 2(b)). Since it is now possible for the gravity current to reach the origin ($x = 0$), we define a critical time t_c at which this occurs; in the present work, t_c is determined from numerical simulations and/or experiments and, in general, could be infinite. Note that, the global mass conservation constraint, as expressed in equation (2.3), no longer holds. Any modification of the latter for flow toward the origin requires the introduction of another length scale x_0 and another time scale t_c into the problem. Therefore, in this physical situation, it is not a priori clear how to obtain a self-similar solution by scaling arguments alone. Moreover, we do not expect complete self-similarity with respect to a similarity variable, i.e., even if a self-similar solution can be obtained it will depend on t_c (or x_0) explicitly (Barenblatt 1952, §5.1.1).

Nevertheless, Darcy's law and the continuity equation still hold, so equation (2.1) remains the governing equation, but the boundary and initial conditions change. In this physical situation, we introduce the phase-plane formalism, following Sedov (1993), Courant & Friedrichs (1999) and Gratton & Minotti (1990), in order to analyze the governing equation. To this end, we substitute the hydrostatic pressure distribution, the gap thickness $b(x) = b_1 x^n$ and the permeability $k(x) = b(x)^2/12$ into equation (2.1) to obtain:

$$u = -\frac{\Delta\rho g b_1^2}{12\mu} x^{2n} \frac{\partial h}{\partial x}, \tag{2.10a}$$

$$\frac{\partial h}{\partial t} + \frac{1}{x^n}\frac{\partial}{\partial x}(x^n h u) = 0. \tag{2.10b}$$

These two equations are the starting point of the phase-plane analysis.

Restricting to the case when $t_c < \infty$, we first introduce $\tau = t_c - t$ as the time remaining to reach the origin ("touch-down"). (Note that if $t_c = \infty$, then we would not be able to make this transformation and proceed with the phase plane analysis. Hence, $t_c = \infty$ corresponds to non-self-similar behavior beyond the scope of the present work.) Then, in order to make equation (2.10) dimensionless, we let

$$u(x,t) = \frac{x}{\tau} U(x,\tau), \qquad h(x,t) = \left(\frac{12\mu}{\Delta\rho g b_1^2}\right) \frac{x^{2(1-n)}}{\tau} H(x,\tau). \tag{2.11a, b}$$

Note that $u \leqslant 0$ for propagation toward the origin and, hence, $U \leqslant 0$ as well; also, $h \geqslant 0$, hence $H \geqslant 0$. Substituting equation (2.11) into equation (2.10), and after some algebra, we obtain the governing equations in terms of the dimensionless variables $H(x,\tau)$ and $U(x,\tau)$:

$$U + x\frac{\partial H}{\partial x} + 2(1-n)H = 0, \tag{2.12a}$$

$$\tau\frac{\partial H}{\partial \tau} - H - x\frac{\partial}{\partial x}(HU) - (3-n)HU = 0. \tag{2.12b}$$

By analogy with other gravity current problems where there is propagation toward the origin (Gratton & Minotti 1990; Diez *et al.* 1992; Angenent & Aronson 1995), we anticipate that we can find a self-similar solution of the second kind. If the flow is to be self-similar, we need to identify a similarity variable. Without loss of generality, we define the similarity variable to be $\xi \equiv x/\tau^\delta$, where δ is to be determined. Then, H and U become functions of only the similarity variable ξ, i.e., $H = H(\xi)$ and $U = U(\xi)$. Thus, for a self-similar flow, equation (2.12) takes the form

$$U + \xi H' + 2(1-n)H = 0, \tag{2.13a}$$

$$\delta\xi H' + H + \xi(HU)' + (3-n)HU = 0. \tag{2.13b}$$

We can eliminate ξ from equation (2.13):

$$\frac{\mathrm{d}U}{\mathrm{d}H} = \frac{H[(n+1)U - 2(1-n)\delta + 1] - U(U+\delta)}{H[2(1-n)H + U]}, \tag{2.14a}$$

$$\frac{\mathrm{d}\ln|\xi|}{\mathrm{d}H} = -\frac{1}{U + 2(1-n)H}. \tag{2.14b}$$

In particular, equation (2.14a) is an autonomous differential equation for the shape of the current. Once $U(H)$ is determined from (2.14a), (2.14b) can be solved to obtain the location of the nose of the current. These steps complete the reduction of the self-similar

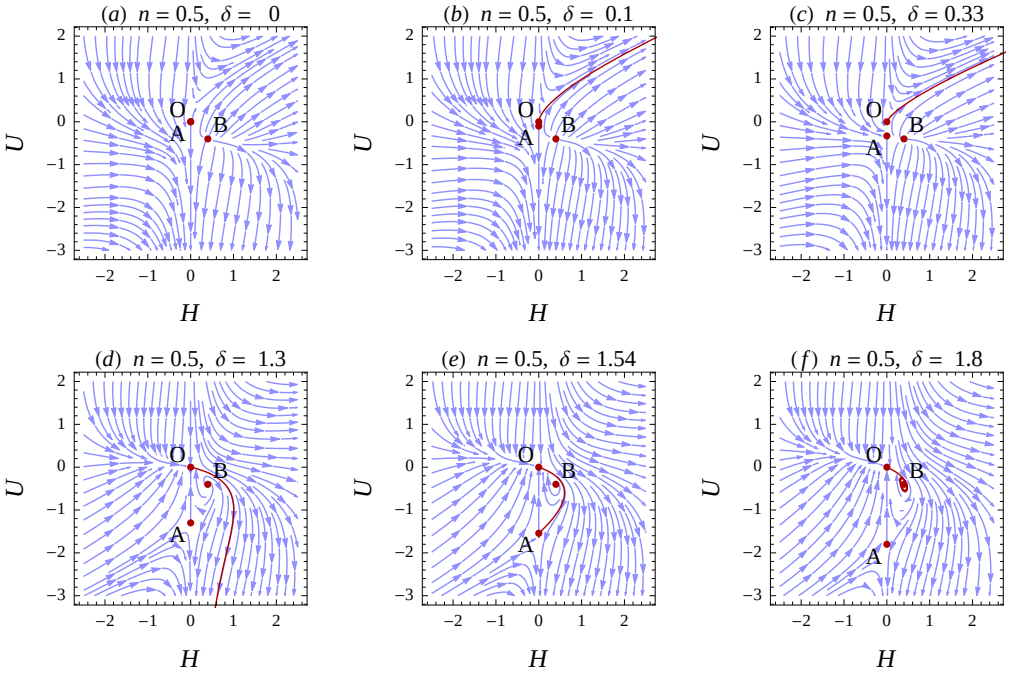

FIGURE 4. Phase portrait of equation (2.14a) with fixed $n = 0.5$ and changing δ (a)-(f). From equation (2.16) we see that $\delta = 0$ (a) is a degenerate case in which point O is no longer a saddle. In panels (b) and (c), the highlighted integral curves (in red) starting at point O in the direction of a neutral eigenvector diverge to infinity. At $\delta = 1/(2-2n)$ ($= 1$ for $n = 0.5$), the neutral eigenvectors flip directions, and now an integral curve starting at point O and passing near point B in the direction of point A exists. At $\delta = \delta_c$, the highlighted integral curve (red) connects point O to point A as shown in panel (e), which means that $\delta = 1.54...$ is the solution δ_c to the nonlinear eigenvalue problem, and the highlighted integral curve $U(H)$ corresponds to a self-similar solution of the second kind. For $\delta > \delta_c$ (f), trajectories starting from point O spiral into point B and, thus, cannot reach point A.

dynamics to a two-dimensional (2D) phase plane (H, U). Different solution (integral) curves in the phase plane represent different flow behaviors, i.e., self-similar solutions of the original PDE. Certain distinguished integral curves of the ordinary differential equation (2.14a) in the phase plane are those that start or end at a critical point and those that form limit cycles. The critical points can be associated with different boundary and initial conditions of the physical system (Gratton & Minotti 1990). We identify the finite critical points of equation (2.14a) by setting its numerator and denominator equal to zero simultaneously to find:

$$\mathrm{O} : (H, U) = (0, 0), \tag{2.15a}$$

$$\mathrm{A} : (H, U) = (0, -\delta), \tag{2.15b}$$

$$\mathrm{B} : (H, U) = \left(\frac{1}{2(1-n)(3-n)}\,, -\frac{1}{3-n} \right). \tag{2.15c}$$

Gratton & Minotti (1990) also considered critical points where $H = \infty$ and/or $U = \infty$, however, this is beyond the scope of the present work.

Point A describes a state of zero current height and finite velocity, which corresponds to the moving front $x_f(t)$ such that $h(x_f(t), t) = 0$ and $dx_f(t)/dt \neq 0$. From the definitions in equation (2.11), we see that point O corresponds to u, h, x and t such that $U = H = 0$.

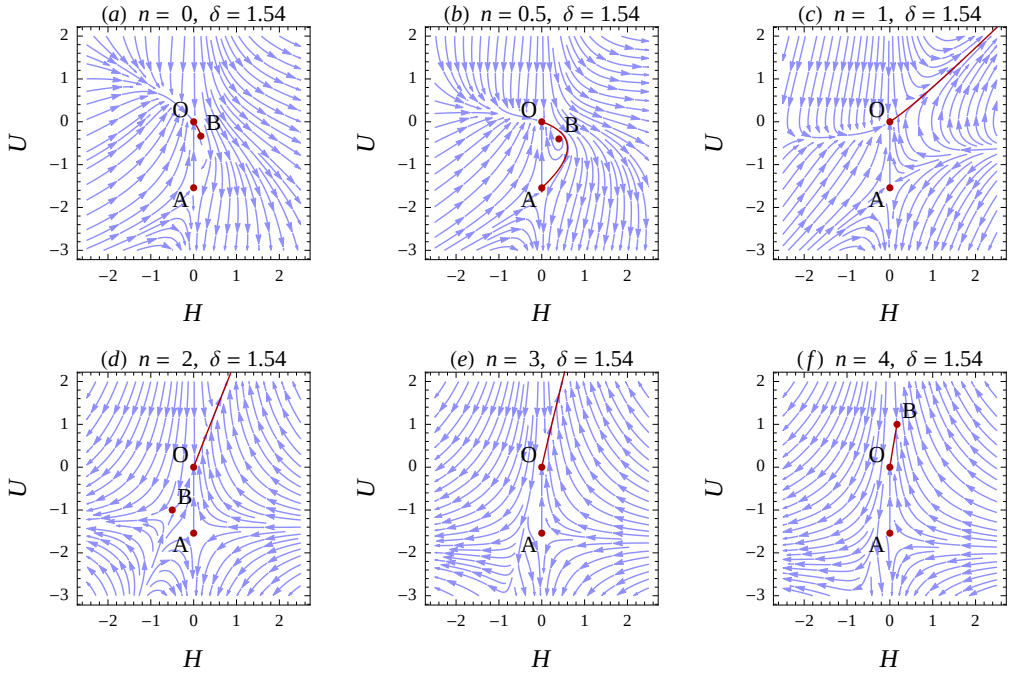

FIGURE 5. Phase portrait with different values of n and $\delta = 1.54$. Changing the value of the parameter n changes the location of the fixed point B, which can lead to the nonlinear eigenvalue problem for δ having no solution. As seen in (c)-(f), a self-similar solution of the second kind, which corresponds to the heteroclinic trajectory from O to A, does not exist for $n \geqslant 1$. Note that, for $n = 1$ and $n = 3$, point B is at infinity, thus it is not shown in panels (c) and (e). The highlighted integral curves (red) start at point O in a neutral eigendirection, $\vec{e}_2$ from equation (2.16).

Suppose, for the sake of argument, that point O does not correspond to the trivial downstream solution: $u = h = 0$ for all x and t. Then, the only way to satisfy equation (2.11) is to set $\tau = 0$. From our definition of τ, we see that this state corresponds to the touch-down time $t = t_c$, when the nose of the gravity current reaches the origin ($x = 0$). Finally, point B does not have a clear physical interpretation in the present context.

Thus, the self-similar solution, which describes a gravity current propagating toward the origin, corresponds to the integral curve connecting O to A in the phase plane. Since δ is still undetermined, it acts as a parameter that allows us to change the phase plane structure until a heteroclinic trajectory from O to A emerges. In other words, we have to solve a nonlinear eigenvalue problem for δ. We do so numerically by a shooting method that we now describe. First, to compute the heteroclinic trajectory, we employ a fundamental-domain technique (Parker & Chua 1989, Chapter 6). To this end, we first note that the linearization of equation (2.14a) at point O shows that it is a degenerate saddle point with the eigenspace:

$$\lambda_1 = -\delta, \qquad \vec{e}_1 = (0, \pm 1), \tag{2.16a}$$

$$\lambda_2 = 0, \qquad \vec{e}_2 = \pm\left(\frac{\delta}{1 - 2(1-n)\delta}, 1\right). \tag{2.16b}$$

Then, we pick two initial conditions (H_i, U_i) that are slight perturbations ($\simeq 10^{-3}$) of point O in the neutral eigendirections given by $\vec{e}_2$, and we integrate (2.14a), which is rewritten as an autonomous system of two ODEs for convenience, numerically in MATHE-

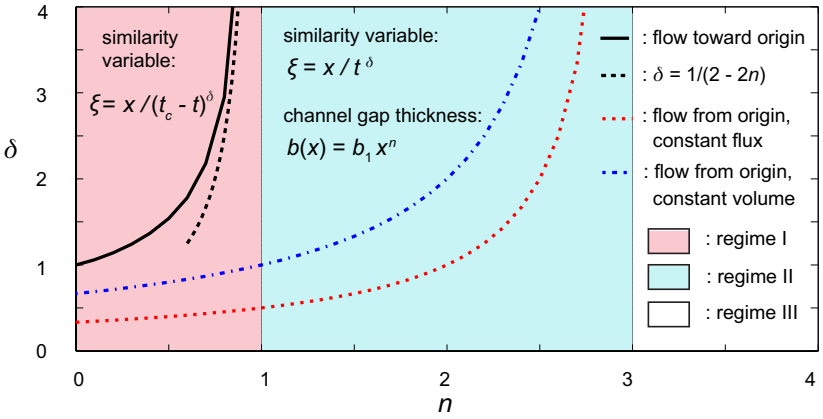

FIGURE 6. Dependence of the exponent of the similarity variable on the gap thickness power-law exponent for various self-similar solutions for viscous gravity currents propagating in a horizontal channel with gap thickness variations in power-law form. For flow from the origin, first-kind self-similar solutions exist in both regime I and regime II; for flow toward the origin, second-kind self-similar solutions exist only in regime I. No self-similar solutions exist in regime III. The exponent δ for the first-kind self-similar solutions was calculated from a scaling argument, see equation (2.4); the exponent δ for the second-kind self-similar solutions was calculated by solving numerically the nonlinear eigenvalue problem described below equation (2.16); the dashed black curve represents the asymptotic behavior of the second-kind self-similar solution's exponent $\delta \sim 1/(2-2n)$ as $n \to 1^-$.

MATICA using the built-in subroutine `NDSolve`. Second, to solve the nonlinear eigenvalue problem, the value of δ is adjusted using a bisection method until the trajectory passes within a prescribed (small $\simeq 10^{-3}$) distance of point A. A visual illustration of this technique is shown in figure 4 for the special case of $n = 0.5$, from which we find that $\delta = 1.54...$. (Note that full double precision, i.e., 16 digits, is required in the value of δ for the heteroclinic trajectory to pass within the prescribed distance of point A and obtain the plot shown in figure 4(e).)

Next, we establish the effect of varying the exponent n that controls the gap thickness of the channel. We study the problem in two ways. First, we show the phase portraits for $\delta = 1.54$ and different n in figure 5. Second, we compute the value of δ numerically for a range of n values, and report the resulting $\delta(n)$ curve in figure 6. For $0 \leqslant n < 1$ (regime I), δ is finite, indicating the existence of a self-similar solution of the second kind. Note that this result also corresponds to point B being in the fourth quadrant ($H > 0, U < 0$) of the (H, U) plane (see figure 5).

Simultaneously, there exists self-similar solutions of the first kind for propagation away from the origin, for which the exponent is given by $(\gamma+1)/(3-n)$ from equation (2.4); the cases $\gamma = 0$ and $\gamma = 1$ correspond to the dashed blue and dashed red curves in figure 6, respectively. In regime II ($1 \leqslant n < 3$), there are only self-similar solutions of the first kind, while the second-kind self-similar solution no longer exists for the currents propagating toward the origin. For $n \geqslant 3$ (regime III), we note again that the first-kind self-similar solution is unphysical.

To better understand the apparently singular behavior of $\delta(n)$ as $n \to 1^-$ in figure 6 for the case of self-similarity of the second kind, we define $\epsilon \equiv 1 - n \to 0^+$. Then, equation (2.14$a$) hints that the eigenvalue $\delta(\epsilon) \sim 1/(2\epsilon)$ as $\epsilon \to 0^+$, which is also supported by the numerics (see figure 6, regime I, dark dashed curve). Meanwhile, we can rescale U and H by the eigenvalue δ, i.e., let $\tilde{H} = H/\delta$ and $\tilde{U} = U/\delta$; for different values of

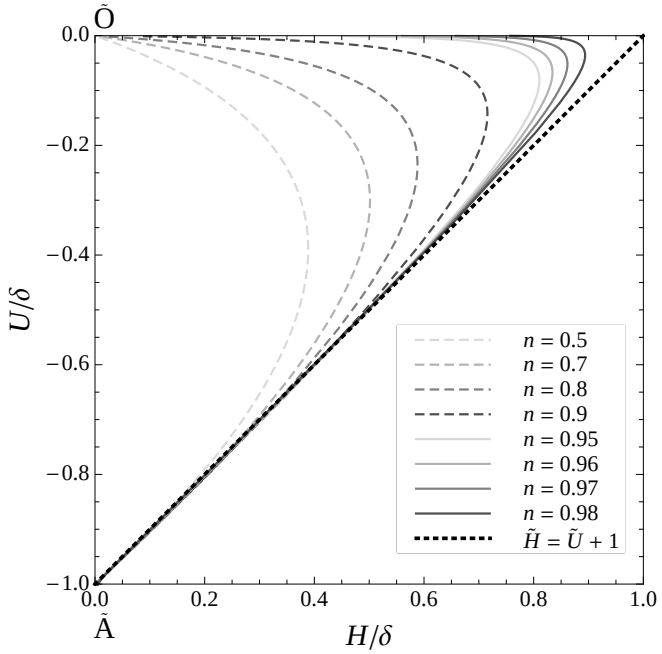

FIGURE 7. Shape of the heteroclinic trajectory of equation (2.14) as $n \to 1^-$ (regime I), in rescaled coordinates. The dotted line represents the asymptotic behavior near point A, i.e., $H \sim U + \delta$.

n, the heteroclinic trajectories, which connect point Ã: $(\tilde{H}, \tilde{U}) = (0, -1)$ and point Õ: $(\tilde{H}, \tilde{U}) = (0, 0)$ in the rescaled coordinates, approach a limiting shape as $n \to 1^-$, as shown in figure 7. Equation (2.14a) can be rewritten in terms of $\tilde{H}$ and $\tilde{U}$; then, near point Ã, which represents the nose of the current, the behavior is given by

$$\frac{\mathrm{d}\tilde{U}}{\mathrm{d}\tilde{H}} = \frac{\tilde{H}[(2-\epsilon)\tilde{U} - 2\epsilon + 1/\delta] - \tilde{U}(\tilde{U}+1)}{\tilde{H}[2\epsilon\tilde{H} + \tilde{U}]} \sim \frac{2\tilde{H} - \tilde{U} - 1}{\tilde{H}} \quad \text{as} \quad \epsilon \to 0^+. \tag{2.17}$$

The latter captures the asymptotic behavior of the heteroclinic trajectory near the nose of the current (point Ã), namely $\tilde{H} \sim \tilde{U} + 1$, shown as the dotted line in figure 7. However, the $\epsilon \to 0^+$ behavior of the ODE does not satisfy the boundary condition near point Õ. A more complete analysis would provide the solution's behavior near point Õ.

It should be noted that when the current is moving toward the origin, the formulation of the nonlinear eigenvalue problem and phase-plane analysis does not make use of the global mass conservation equation (2.3). Therefore, the injection rate $\gamma Q t^{\gamma-1}$ does not affect the existence of second-kind self-similar solutions. However, Q and γ may affect the validity of the model assumptions by changing the aspect ratio of the gravity current; in particular, $|\partial h/\partial x| \ll 1$ (lubrication) may fail to hold or the drag at the bottom plate may become important if $h = O(b)$ throughout most of the current. In either case, the values of Q and γ will change the initial transition period before the gravity current's propagation becomes self-similar in this case.

2.2. *Gravity currents in heterogeneous porous media*

In this subsection, we consider a related problem: the propagation of gravity currents in heterogeneous porous media in which the permeability and porosity follow power laws in the horizontal direction. We place the origin at the location where the permeability and

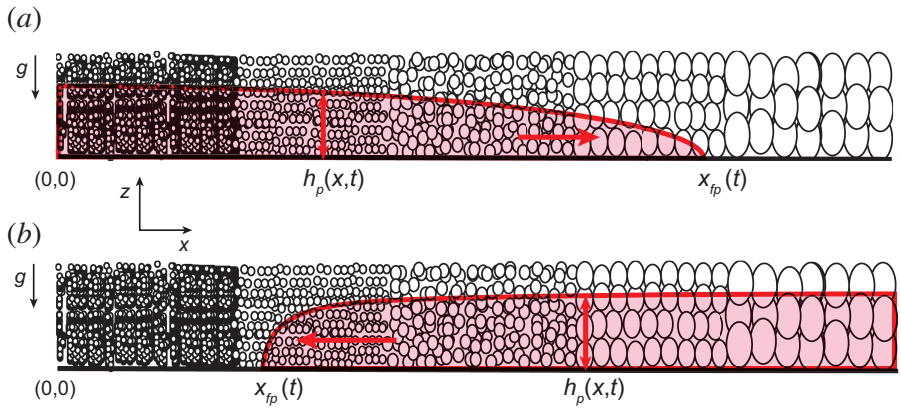

FIGURE 8. Diagram of gravity currents propagating along a horizontal boundary in heterogeneous porous media with power-law permeability $k_p(x) = k_1 x^n$ and porosity $\phi_p(x) = \phi_1 x^m$ variations, which give rise to gradients in the horizontal direction. (*a*) A gravity current propagating away from the origin in the direction of increasing permeability and porosity. (*b*) A gravity current propagating toward the origin from far away. Gravity is directed in the negative z-direction as before; $h_p(x,t)$ and $x_{fp}(t)$ represent the shape and location of the nose of the current, respectively.

porosity vanish, as shown in figure 8. Then, the permeability and porosity are given by $k_p(x) = k_1 x^n$ and $\phi_p(x) = \phi_1 x^m$, respectively, where k_1, ϕ_1, n and m are non-negative real numbers, and x is the streamwise coordinate as before. Generally, n and m are not independent of each other. In practice, $2 < n/m < 3$, where $n/m = 2$ corresponds to the extreme case of a porous medium composed of tubular pores, while $n/m = 3$ corresponds to a porous medium composed of an network of intersecting fissures (Phillips 1991; Dullien 1992).

As before, we assume the two fluids are immiscible but we neglect surface tension effects. We also assume the current is long and thin, so the flow is mainly in the horizontal direction, and we neglect any motion in the displaced fluid. For clarity, the variables in this subsection are appended with the subscript "p". However, note that n still denotes the exponent in the assumed power-law variation of the permeability, just as in the Hele-Shaw case in §2.1, but the expressions for $k(x)$ and $k_p(x)$ are not identical.

2.2.1. *Flow away from the origin*

When the gravity current is propagating horizontally from the origin to regions of higher permeability and porosity, we once again start from Darcy's law and the local continuity equation, which now take the form

$$u_p = -\frac{k_p(x)}{\mu}\frac{\partial p}{\partial x}, \tag{2.18a}$$

$$\phi_p(x)\frac{\partial h_p}{\partial t} + \frac{\partial}{\partial x}(h_p u_p) = 0. \tag{2.18b}$$

Substituting the hydrostatic pressure distribution, the posited permeability and porosity expressions, and combining the two equations in (2.18), we obtain a nonlinear diffusion

equation for the shape $h_p(x,t)$ of the gravity current:

$$\frac{\partial h_p}{\partial t} - \frac{A_p}{x^m}\frac{\partial}{\partial x}\left(x^n h_p \frac{\partial h_p}{\partial x}\right) = 0, \tag{2.19}$$

where $A_p = (\Delta\rho g k_1)/(\mu\phi_1)$. The global mass conservation constraint takes the form

$$\int_0^{x_{fp}(t)} x^m h_p(x,t)\,\mathrm{d}x = B_p t^\gamma, \tag{2.20}$$

where, similar to before, $B_p = Q_p/\phi_1$, and $\gamma Q_p t^{\gamma-1}$ is the injection rate. For clarity, we now denote the front position as $x_{fp}(t)$, where $h_p\left(x_{fp}(t),t\right) = 0$.

As in §2.1, through a scaling analysis of equations (2.19) and (2.20), we find a similarity variable

$$\xi = \frac{x}{(AB)^{1/(2m-n+3)}t^{(\gamma+1)/(2m-n+3)}}. \tag{2.21}$$

Then, the location of the nose of the current is given by

$$x_{fp}(t) = \xi_{fp}(m,n,\gamma)(AB)^{\frac{1}{2m-n+3}}t^{\frac{\gamma+1}{2m-n+3}}, \tag{2.22}$$

In terms of the similarity variable, the shape of the current is given by

$$h_p(x,t) = \xi_{fp}^{m-n+2}A^{-\frac{m+1}{2m-n+3}}B^{\frac{m-n+2}{2m-n+3}}t^{\frac{(m-n+2)\gamma-(m+1)}{2m-n+3}}f_p(y), \tag{2.23}$$

where $y \equiv x/x_{fp}(t) = \xi(x,t)/\xi_{fp}(m,n,\gamma)$. Then, $f_p(y)$ and $\xi_{fp}(m,n,\gamma)$ are obtained by solving the following system:

$$(y^n f_p f_p')' + \left(\frac{\gamma+1}{2m-n+3}\right)y^{m+1}f_p' - \left(\frac{(m-n+2)\gamma-(m+1)}{2m-n+3}\right)y^m f_p = 0, \tag{2.24a}$$

$$f_p(1) = 0, \tag{2.24b}$$

$$\xi_{fp}(m,n,\gamma) = \left(\int_0^1 y^m f_p(y)\,\mathrm{d}y\right)^{1/(n-2m-3)}. \tag{2.24c}$$

For $n = 3m$, equation (2.24) reduces to equation (2.7) with n replaced by m. Also, when $m = n = 0$, equation (2.24) reduces to the homogeneous porous medium case in Cartesian coordinates, as above. Meanwhile, when $m = n = 1$, equation (2.24a) reduces to the equation for homogeneous case in axisymmetric coordinates (Lyle *et al.* 2005).

Again, we can determine the asymptotic behavior of the current near the nose from (2.24a,b):

$$f_p(y) \sim \left(\frac{\gamma+1}{2m-n+3}\right)(1-y) \quad \text{as} \quad y \to 1^-, \tag{2.25}$$

which provides two boundary conditions near $y = 1$, i.e., $f_p(1-\nu)$ and $f_p'(1-\nu)$, $\nu \ll 1$, in a shooting procedure for solving equation (2.24a) numerically. Typical shapes, $f_p(y)$, of the current are show in figure 9 for (a) constant volume ($\gamma = 0$) and (b) constant injection rate ($\gamma = 1$) and various choices of m and n. The dependence of ξ_{fp} on γ is illustrated in figure 9(c) for various choices of m and n.

For $\gamma = 0$ and $0 \leqslant n < 2m+3$, it can be shown that equation (2.24) possesses the

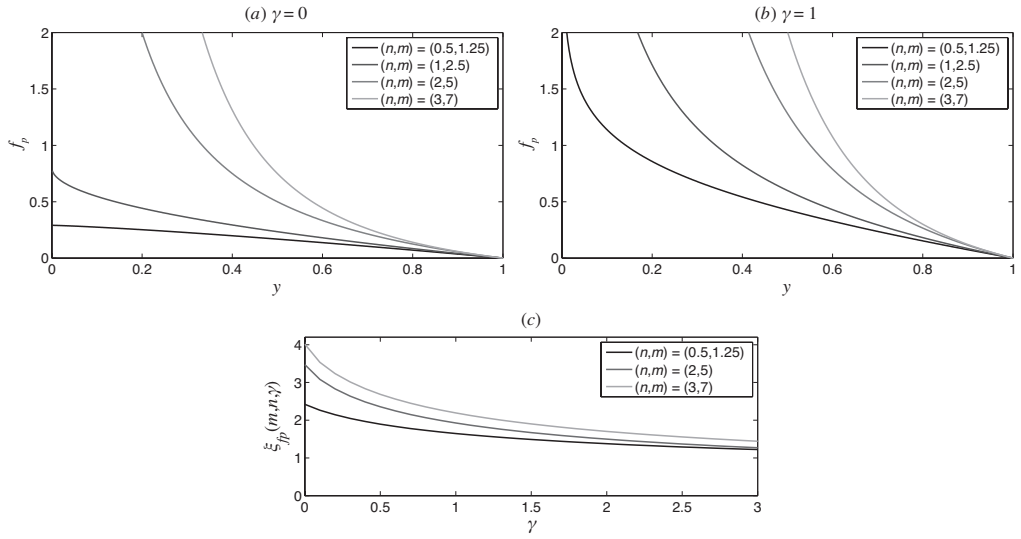

FIGURE 9. Self-similar shape of a viscous gravity current propagating away from the origin in a heterogeneous porous medium with variable permeability $k_p(x) = k_1 x^n$ and porosity $\phi_p(x) = \phi_1 x^m$ for (a) constant volume and (b) constant injection rate, and various choices of n and m; the pre-factor $\xi_{fp}(m, n, \gamma)$ is shown in panel (c). The solutions for f_p were found by integrating equation (2.24) numerically by shooting backwards from $y = 1 - \nu$ ($\nu = 10^{-4}$), where boundary conditions on f_p and f_p' are imposed using the asymptotic form given from equation (2.25).

exact solution

$$f_p(y) = \begin{cases} \dfrac{1}{(m-n+2)(2m-n+3)}\left(1 - y^{m-n+2}\right), & n \neq m+2, \\ -\dfrac{1}{m+1}\ln y, & n = m+2, \end{cases} \tag{2.26a}$$

$$\xi_{fp}(m, n, 0) = \left[(m+1)(2m-n+3)^2\right]^{1/(2m-n+3)}. \tag{2.26b}$$

2.2.2. *Flow toward the origin*

When the gravity current is moving horizontally toward the origin, i.e., in the direction from higher to lower permeability, in a porous medium, equation (2.18) still holds. However, as above, we cannot determine the self-similar solution by scaling alone, so we introduce a phase-plane analysis to seek a second-kind similarity solution. We begin with equation (2.18), i.e., the coupled equations for the transversely averaged fluid velocity and continuity. First, we substitute in the hydrostatic pressure distribution, the permeability and porosity expressions into equation (2.18) to obtain

$$u_p = -\frac{\Delta\rho g k_1 x^n}{\mu}\frac{\partial h_p}{\partial x}, \tag{2.27a}$$

$$\frac{\partial h_p}{\partial t} + \frac{1}{\phi_1 x^m}\frac{\partial (h_p u_p)}{\partial x} = 0. \tag{2.27b}$$

Again, assuming $t_c < \infty$, we let $\tau = t_c - t$ and, then, introduce dimensionless variables via

$$u_p(x,t) = \phi_1 \frac{x^{m+1}}{\tau} U_p(x,\tau), \qquad h_p(x,t) = \left(\frac{\mu\phi_1}{\Delta\rho g k_1}\right)\frac{x^{m-n+2}}{\tau} H_p(x,\tau). \tag{2.28a, b}$$

Substituting the latter into equation (2.27), we obtain

$$U_p + x\frac{\partial H_p}{\partial x} + (m-n+2)H_p = 0, \tag{2.29a}$$

$$\tau\frac{\partial H_p}{\partial \tau} - H_p - x\frac{\partial (H_pU_p)}{\partial x} - (2m-n+3)H_pU_p = 0. \tag{2.29b}$$

Now, if the flow is to be self-similar, we should be able to reduce the x and t dependence to dependence on a single similarity variable $\xi \equiv x/\tau^{\delta}$, where δ remains to be determined, so that H_p and U_p become functions of ξ alone. Under this assumption, equation (2.29) becomes

$$U_p + \xi H_p' + (m-n+2)H_p = 0, \tag{2.30a}$$

$$\delta\xi H_p' + H_p + \xi(H_pU_p)' + (2m-n+3)H_pU_p = 0. \tag{2.30b}$$

Finally, we eliminate ξ from equation (2.30) to find

$$\frac{\mathrm{d}U_p}{\mathrm{d}H_p} = \frac{H_p[(m+1)U_p - (m-n+2)\delta + 1] - U_p(U_p+\delta)}{H_p[(m-n+2)H_p + U_p]}, \tag{2.31a}$$

$$\frac{\mathrm{d}\ln|\xi|}{\mathrm{d}H_p} = -\frac{1}{U_p + (m-n+2)H_p}. \tag{2.31b}$$

Thus, we have constructed the phase plane (H_p, U_p) for a gravity current propagating toward the origin in a heterogeneous porous medium. Equation (2.31a) has three finite critical points:

$$\mathrm{O} : (H_p, U_p) = (0,0), \tag{2.32a}$$

$$\mathrm{A} : (H_p, U_p) = (0, -\delta), \tag{2.32b}$$

$$\mathrm{B} : (H_p, U_p) = \left(\frac{1}{(m-n+2)(2m-n+3)}\,, -\frac{1}{2m-n+3}\right). \tag{2.32c}$$

As in §2.1.2, when the current is propagating toward the origin, the integral curve that connects point O to point A corresponds to the similarity solution of the second kind. Depending on the values of n and m, we can numerically determine the value of δ using the numerical technique outlined after equation (2.16), where the linearized eigenspace at point O is now

$$\lambda_1 = -\delta, \qquad \vec{e}_1 = (0, \pm 1), \tag{2.33a}$$

$$\lambda_2 = 0, \qquad \vec{e}_2 = \pm\left(\frac{\delta}{1-(2+m-n)\delta}\,, 1\right). \tag{2.33b}$$

The types of self-similar solutions that can be expected on the basis of this analysis are summarized in figure 10, in which we color different regions of the (m,n) plane to illustrate the possible behaviours. As noted earlier, $n/m = 2$ and $n/m = 3$ correspond to two limiting cases of the porous medium's microstructure. Restricting ourselves only to (m,n) such that $2 < n/m < 3$, self-similar solutions are to be expected in the wedge $2m < n < 3m$ as shown by the dashed lines in figure 10. Furthermore, for $n < m+2$, we see from equation (2.32c) that point B is in the fourth quadrant of the (H_p, U_p) phase plane, thus we expect second-kind self-similar solutions in this region (regime I) of the (m,n) plane. The region in which $m+2 < n < 2m+3$ (in addition to $2m < n < 3m$) is denoted as regime II, in which we only expect self-similar solutions of the first kind. The latter are advancing fronts because the exponent of t in equation (2.22) is positive for

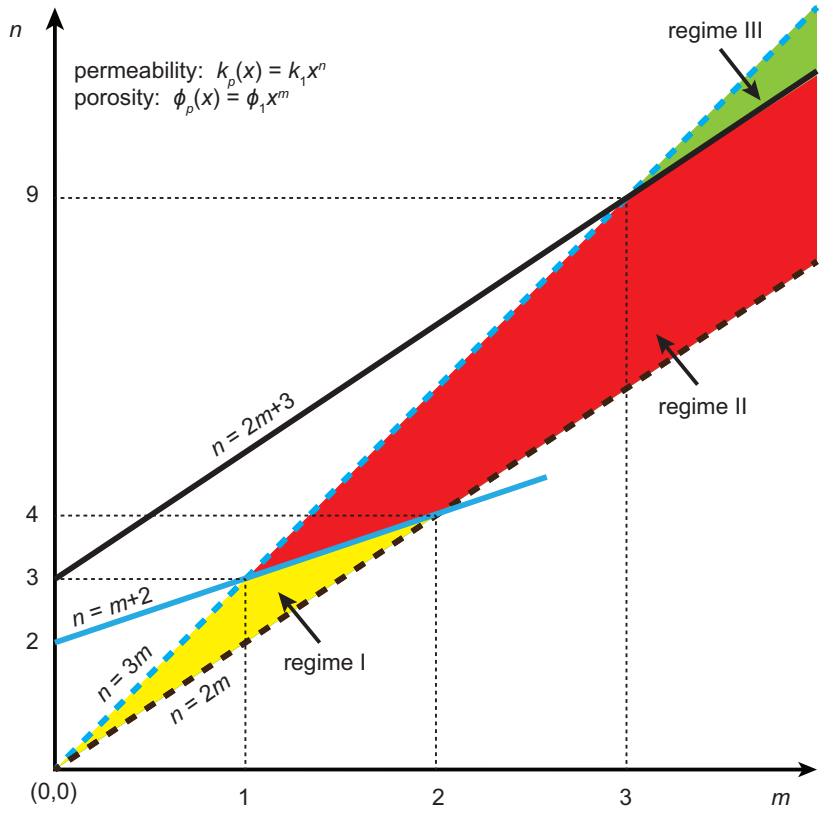

FIGURE 10. Flow regimes for gravity currents propagation in heterogeneous porous media with power-law permeability $k_p(x) = k_1 x^n$ and porosity $\phi_p(x) = \phi_1 x^m$ variations in the horizontal direction. When a gravity current is propagating toward the origin, a self-similar solution exists only in regime I, and it is of the second kind. When a gravity current is propagating away from the origin, a first kind self-similar solution is found in both regimes I and II. In regime III, there are neither advancing nor physically meaningful self-similar solutions.

(m, n) in this regime. Finally, for $n > 2m + 3$ (regime III), there are no advancing first-kind self-similar solutions, and, moreover, the first-kind self-similar solution is unphysical because it predicts $f_p < 0$. This classification is analogous to that in figure 6.

3. Results from experiments and numerical simulation

We conducted a series of constant-volume gravity current experiments in horizontal Hele-Shaw cells whose gap thicknesses vary as power laws of the streamwise coordinate. We also solved the corresponding governing partial differential equation (2.2), which we derived above under the lubrication approximation. The numerical scheme is described in Appendix B. In this section, we present a discussion of and a comparison between the experiments, numerical simulations and the theoretical considerations from self-similar intermediate asymptotics for the case of a gravity current propagating toward the origin of a horizontal channel.

We designed three Hele-Shaw cells with different power-law shapes: (a) $n = 0.2$, (b) $n = 0.5$, and (c) $n = 0.8$; recall figure 2. The cells were constructed from scratch-resistant clear cast acrylic sheets (McMaster-Carr, No. 8560K247) using an automatic

experiment	liquid (% glycerol)	n	b_1 (m^{1-n})	L_{cell} (m)	x_0 (m)	w (kg)	t_c (s)
#1	100%	0.2	0.01589	0.75	0.560	0.1489	86.0
#2	100%	0.2	0.01589	0.75	0.550	0.1569	66.1
#3	100%	0.2	0.01589	0.75	0.550	0.1480	78.7
#4	100%	0.5	0.01732	0.75	0.575	0.1731	89.0
#5	100%	0.5	0.01732	0.75	0.578	0.1602	104.1
#6	95%	0.5	0.01732	0.75	0.578	0.1559	54.9
#7	95%	0.5	0.01732	0.75	0.600	0.1228	76.7
#8	90%	0.5	0.01732	0.75	0.585	0.1556	23.0
#9	90%	0.5	0.01732	0.75	0.581	0.1574	22.3
#10	100%	0.8	0.03776	0.75	0.530	0.3169	81.5
#11	100%	0.8	0.03776	0.75	0.515	0.3494	64.5
#12	100%	0.8	0.03776	0.75	0.525	0.2464	102.5

TABLE 1. Summary of the parameters of the different experiments that we performed of viscous gravity currents propagating toward the origin of a horizontal channel. Glycerol–water solutions were used with various glycerol mass concentrations, as shown in the second column. The gap thickness of the horizontal channel is given by $b(x) = b_1 x^n$, L_{cell} is the total length of the channel, x_0 is the location of the lock gate, w is the total weight of the liquid in the cell, and t_c is the time when the moving front reaches the origin in an experiment.

manufacturing machine. The liquids we used were glycerol–water solutions with various glycerol concentrations, whose physical properties were looked up in published tables. The glycerol is colored with food dye so the profile shapes of the liquid can be recorded at different times using a USB camera.

We begin each experiment by setting up a lock gate at a certain location $x = x_0$ from the origin, where x_0 was chosen near the end of the channel ($x = L_{cell}$) to allow for a larger distance over which the gravity current can propagate. We then filled the gap between the lock and the end with the glycerol–water solution and suddenly removed the lock gate, allowing the fluid to propagate toward the origin ($x = 0$). We recorded the location of the propagating front $x_f(t)$ at different times.

Details of different experimental designs are summarized in Table 1. In these experiments, we can vary different parameters: (*a*) the gap thickness; (*b*) the glycerol concentration, thus the viscosity and density of the fluid; (*c*) the location x_0 of the lock gate; and (*d*) the initial volume of liquid placed behind the lock gate. To justify the lubrication approximation utilized in §2, we estimate the product of the aspect ratio and the Reynolds number: the typical channel width is given by $b_1 x_0^n$, the typical length scale is x_0, the velocity scale is x_0/t_c, where t_c is the time for the front to reach the origin, ρ and μ are the density and viscosity, respectively, of the glycerol solution ($\rho = 1,261$ $\mathrm{kg/m^3}$ and $\mu = 1.412$ Pa s for 100% glycerol). Thus, for a typical experiment (e.g., experiment #1 in table 1), the product of the aspect ratio and Reynolds number is $\rho b_1^2 x_0^{2n}/(\mu t_c) \approx 2 \times 10^{-3} \ll 1$. Also, in a typical experiment, $h/b > 3$ for most of the current (i.e., except at the nose), therefore, drag due to the bottom plate can be neglected. Furthermore, in a typical experiment, the gap thickness b is such that $b(x) > 3$ mm, which is the capillary length for the fluids we use, for 3 cm $< x < L_{cell} = 75$ cm, i.e., for

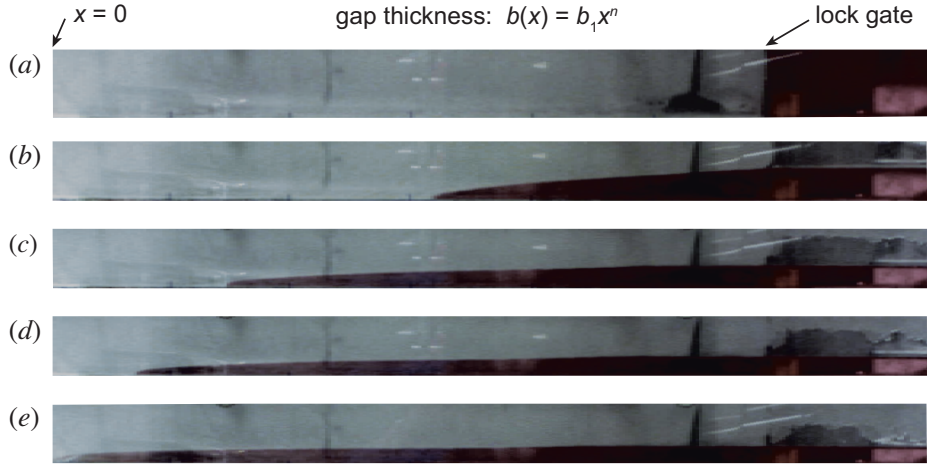

FIGURE 11. Time-lapse images of a viscous gravity current (experiment #8 from the Table 1) propagating toward the origin of a horizontal channel (as in figures 1(d) and 2(b)) at (a) $t = 0$ s, (b) $t = 1.5$ s, (c) $t = 6.5$ s,(d) $t = 11.5$ s, and (e) $t = t_c \approx 22.3$ s, which is when the front is observed to reach the origin ($x_f(t_c) = 0$). The flow was generated by an instantaneous removal of a vertical lock gate. Contrast has been digitally enhanced for visual clarity.

96% of the length of the Hele-Shaw cell. Therefore, surface tension can be neglected as well. The fact that drag due to the bottom plate and surface tension can potentially be important near the nose of the current does not affect its global self-similar behavior, as is evidenced by our experiments and those in the literature.

For Hele-Shaw cells with $n < 1$, we measured a finite critical time t_c at which the front reaches the origin. In figure 12, we plot the rescaled front location $x_f(t)/x_0$ versus the dimensionless time-to-touchdown $\tau/t_c = 1 - t/t_c$ for different experimental conditions. The assumption of self-similarity of the second kind leads us to expect that $x_f(t)/x_0 \propto (1-t/t_c)^\delta$. Numerical simulation results for $x_f(t)/x_0$ are also plotted on the same figure. As can be seen in figure 12, the experimental results agree very well with the numerical simulation for all of the geometries considered. In particular, as the front approaches the origin, i.e., as $1 - t/t_c \to 0^+$, the initial shape of the current is forgotten, and both the experimental and numerical simulation data for the rescaled location of the nose of the current versus dimensionless time-to-touch-down fall on a straight line in this log-log plot. Therefore, the behavior is self-similar, as we predicted in our theoretical discussion in §2.1.2. Furthermore, the values that the slopes of the curves asymptote to agree very well with the predictions from the theory, namely, $\delta \approx 1.14$ for $n = 0.2$, $\delta \approx 1.54$ for $n = 0.5$, and $\delta \approx 2.95$ for $n = 0.8$, where these slopes are predicted via the second-kind phase-plane analysis (recall figure 4 and its discussion).

4. Summary and conclusions

In this paper, we investigated the effects of horizontal heterogeneity on the propagation of viscous gravity currents, with an emphasis on second-kind self-similar behavior. Two geometries were studied in detail as illustrative examples: (a) horizontal channels or cracks with a varying gap thickness of power-law form and (b) heterogeneous porous media with power-law permeability and porosity variations. In each case, two flow patterns were considered: (a) gravity currents propagating away from the origin (defined

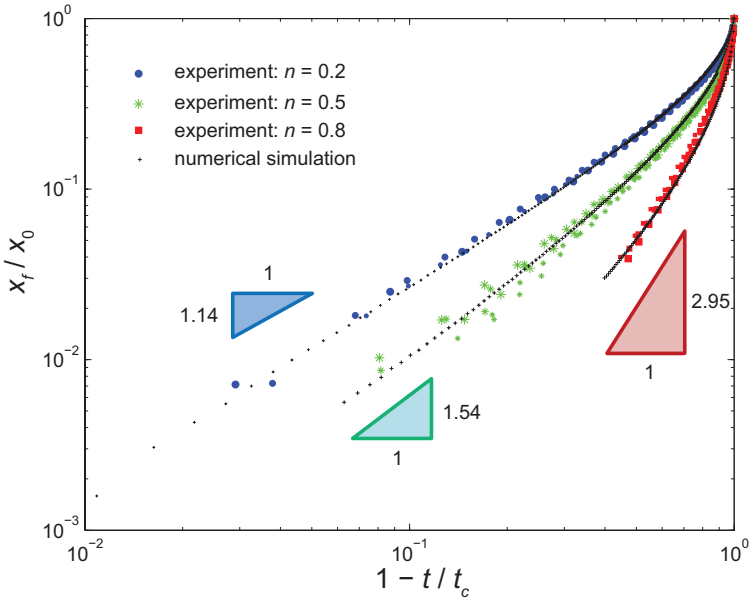

FIGURE 12. Constant-volume gravity currents propagating in Hele-Shaw cells with gap thicknesses of power-law form: $b(x) = b_1 x^n$. Comparison of experiments and numerical simulations for propagation toward the origin. Experiments in three different Hele-Shaw cells were performed: $n = 0.2$ (circles), $n = 0.5$ (stars) and $n = 0.8$ (squares). In both experiments and numerical simulations (crosses), self-similar solutions of the second kind were observed for the three different geometries and the similarity exponents (i.e., the intermediate asymptotic slope on the plot) are in good agreement with the theory (large triangles).

as the point of vanishing permeability) and (b) gravity currents propagating toward the origin.

We employed experimental, theoretical and numerical techniques to study the flow behavior. Our key findings are: (i) when a viscous gravity current propagates away from the origin in this heterogeneous medium, the behavior is described by self-similar solution of the first kind, as is to be expected based on similar problems in the literature; (ii) when the current propagates toward the origin in these models with horizontal heterogeneity, the behavior is described by self-similarity of the second kind with a nontrivial exponent in the similarity variable. Depending on the form of the heterogeneity, different flow regimes are identified corresponding to the existence of either first-kind or both first- and second-kind self-similarity.

Our study may have possible connections to industrial processes and geological flows in porous media, including recent applications in geological CO_2 storage (see, e.g., Class *et al.* 2009; Zheng *et al.* 2010) and shale gas recovery (see, e.g., Monteiro *et al.* 2012). For example, in the presence of horizontal heterogeneity, the propagation regime of a CO_2 plume can change. In the case of shale gas recovery, the propagation of a gas driven by buoyancy in the horizontal channels created by hydraulic fracturing is affected by the shape of the passage. Our study presents and benchmarks a possible theoretical approach to understanding the various flow regimes in a certain class of fissure shapes in a porous medium or crack shapes in a reservoir. Specifically, we show how to obtain the various self-similar behaviors, even for the cases where scaling alone cannot reveal such dynamics.

Acknowledgements

We thank the Princeton Carbon Mitigation Initiative for support of this research, N. Hammoud and R. H. Socolow for helpful conversations. I.C.C. was supported by the National Science Foundation (NSF) under Grant No. DMS-1104047 (at Princeton University) and by the LANL/LDRD Program through a Feynman Distinguished Fellowship (at Los Alamos National Laboratory); he thanks C. I. Christov for advice on the construction of the numerical scheme. LANL is operated by Los Alamos National Security, L.L.C. for the National Nuclear Security Administration of the U.S. Department of Energy under Contract No. DE-AC52-06NA25396.

Appendix A. Phase plane formalism for gravity currents propagating toward the origin in a homogeneous porous medium

A.1. *Axisymmetric gravity currents in a homogenous porous medium*

Second-kind self-similar solutions also exist for axisymmetric gravity currents propagating in homogeneous porous media (i.e., constant permeability k and porosity ϕ) as depicted in figure 1(b). We denote the shape of the gravity current by $h_a(r,t)$ and its propagation velocity by $u_a(r,t)$, as before, then Darcy's Law and the continuity equation are

$$u_a = -\frac{\Delta\rho g k}{\mu}\frac{\partial h_a}{\partial r}, \tag{A 1a}$$

$$\phi\frac{\partial h_a}{\partial t} + \frac{1}{r}\frac{\partial}{\partial r}\left(r h_a u_a\right) = 0, \tag{A 1b}$$

respectively. Following the procedure from the earlier sections, for $t_c < \infty$, we let $\tau = t_c - t$ and

$$u_a(r,t) = \phi\frac{r}{\tau}U_a(r,\tau), \qquad h_a(r,t) = \left(\frac{\mu\phi}{\Delta\rho g k}\right)\frac{r^2}{\tau}H_a(r,\tau). \tag{A 2a, b}$$

If the flow is to be self-similar, then U_a and H_a should depend solely on a similarity variable $\xi \equiv r/\tau^\delta$, hence equation (A 1) becomes

$$\frac{\mathrm{d}U_a}{\mathrm{d}H_a} = \frac{H_a(2U_a - 2\delta + 1) - U_a(U_a + \delta)}{H_a(2H_a + U_a)}, \tag{A 3a}$$

$$\frac{\mathrm{d}\ln|\xi|}{\mathrm{d}H_a} = -\frac{1}{U_a + 2H_a}. \tag{A 3b}$$

We note that equation (A 3) corresponds to the nonlinear heat conduction problem described in equation (15) of Gratton & Minotti (1990) with $m = n = 1$ (in their notation).

Equation (A 3a) has three finite critical points:

$$\mathrm{O} : (H_a, U_a) = (0, 0), \tag{A 4a}$$

$$\mathrm{A} : (H_a, U_a) = (0, -\delta), \tag{A 4b}$$

$$\mathrm{B} : (H_a, U_a) = \left(\frac{1}{8}\,,\, -\frac{1}{4}\right). \tag{A 4c}$$

A second-kind self-similar solution is found for $\delta = \delta_c$ such that there exist a heteroclinic orbit from point O to point A in the phase plane. Since point B is in the fourth quadrant in this physical situation, and there are no parameters in this model, there always exist both first- and second-kind self-similar solutions.

A.2. *Gravity currents in a homogenous porous medium with converging boundaries*

Second-kind self-similar solutions also exist for a viscous gravity current propagating in a homogeneous porous medium (i.e., constant permeability k and porosity ϕ) with converging boundaries of power-law form $b_c(x) = b_{c1}x^n$ as depicted in figure 1(d). We denote the shape of the gravity current by $h_c(x,t)$ and its propagation velocity by $u_c(x,t)$, then Darcy's Law and the continuity equation are

$$u_c = -\frac{\Delta\rho g k}{\mu}\frac{\partial h_c}{\partial x}, \tag{A 5a}$$

$$\phi\frac{\partial h_c}{\partial t} + \frac{1}{x^n}\frac{\partial}{\partial x}\left(x^n h_c u_c\right) = 0, \tag{A 5b}$$

respectively. Again, following the same procedure as before, for $t_c < \infty$, we let $\tau = t_c - t$ and

$$u_c(x,t) = \phi\frac{x}{\tau}U_c(x,\tau), \qquad h_c(x,t) = \left(\frac{\mu\phi}{\Delta\rho g k}\right)\frac{x^2}{\tau}H_c(x,\tau). \tag{A 6a, b}$$

If the flow is to be self-similar, H_c and U_c depend only on a similarity variable $\xi \equiv x/\tau^\delta$, hence equation (A 5) becomes

$$\frac{\mathrm{d}U_c}{\mathrm{d}H_c} = \frac{H_c[(n+1)U_c - 2\delta + 1] - U_c(U_c+\delta)}{H_c(2H_c+U_c)}, \tag{A 7a}$$

$$\frac{\mathrm{d}\ln|\xi|}{\mathrm{d}H_c} = -\frac{1}{U_c+2H_c}. \tag{A 7b}$$

Equation (A 7a) has three finite critical points:

$$\mathrm{O} : (H_c, U_c) = (0,0), \tag{A 8a}$$

$$\mathrm{A} : (H_c, U_c) = (0,-\delta), \tag{A 8b}$$

$$\mathrm{B} : (H_c, U_c) = \left(\frac{1}{2(n+3)}, -\frac{1}{n+3}\right). \tag{A 8c}$$

A second-kind self-similar solution exists for $\delta = \delta_c$ such that there exist a heteroclinic orbit from point O to point A in the phase plane. We expect that both first- and second-kind self-similar solutions exist for all n, since point B is in the fourth quadrant for all n in this physical situation.

Appendix B. Numerical scheme for nonlinear diffusion equations with spatially varying coefficients

B.1. *Preliminaries*

In this section, we develop a new finite-difference numerical method capable of handling the nonlinear parabolic PDEs that arise in this work. To this end, let us use the following notation for the purposes of this section:

$$\frac{\partial h}{\partial t} = \frac{A}{x^p}\frac{\partial}{\partial x}\left(x^q h^s \frac{\partial h}{\partial x}\right), \qquad (x,t) \in (0,L)\times(0,t_f). \tag{B 1}$$

Here, A, p, q and s are positive real numbers; for example, $p = n$, $q = 3n$ and $s = 1$ gives equation (2.2), while $h = h_p$, $A = A_p$, $p = m$, $q = n$ and $s = 1$ gives equation (2.19). In general, p and q are not arbitrary, but determined by the physics at hand. L is the size of the computational domain, and t_f is the final time in the simulation.

Rather than solving a moving boundary-value problem on $(0, x_f(t))$, we prefer to solve the problem numerically on a fixed domain $(0, L)$ and impose appropriate boundary conditions at $x = 0$ and $x = L$ to automatically enforce the global mass conservation constraint from, e.g., equation (2.3). To establish the appropriate boundary conditions, we begin by multiplying equation (B 1) by x^p and integrating from $x = 0$ to $x = L$:

$$\frac{\mathrm{d}}{\mathrm{d}t}\int_0^L x^p h(x,t)\,\mathrm{d}x = A\left[x^q h^s \frac{\partial h}{\partial x}\right]_0^L. \tag{B 2}$$

Now, we enforce the constraint on the total mass by noting that $h(x,t) = 0$ for $x \geqslant x_f(t)$, hence $\int_0^{x_f} x^p h\,\mathrm{d}x = \int_0^L x^p h\,\mathrm{d}x = Bt^\gamma \Rightarrow \frac{\mathrm{d}}{\mathrm{d}t}\int_0^L x^p h\,\mathrm{d}x = \gamma B t^{\gamma-1}$ ($\gamma \neq 0$). Now, we require that

$$A\left[x^q h^s \frac{\partial h}{\partial x}\right]_0^L \equiv AL^q \left(h^s h_x\right)\Big|_{x=L} - A\left(x^q h^s h_x\right)\Big|_{x\to 0} = \begin{cases} \gamma B t^{\gamma-1}, & \gamma \neq 0, \\ 0, & \gamma = 0. \end{cases} \tag{B 3}$$

Assuming injection from a single boundary, we can derive two sets of BCs for the PDE from equation (B 3):

$$\left(x^q h^s h_x\right)\big|_{x\to 0} = \begin{cases} -\frac{\gamma B}{A} t^{\gamma-1}, & \gamma \neq 0, \\ 0, & \gamma = 0, \end{cases} \tag{B 4a}$$

$$\left(h^s h_x\right)\big|_{x=L} = 0 \quad \Rightarrow \quad h_x\big|_{x=L} = 0, \tag{B 4b}$$

and

$$\left(x^q h^s h_x\right)\big|_{x\to 0} = 0 \quad \Rightarrow \quad h_x\big|_{x=0} = 0, \tag{B 5a}$$

$$\left(h^s h_x\right)\big|_{x=L} = \begin{cases} \frac{\gamma B}{AL^q} t^{\gamma-1}, & \gamma \neq 0, \\ 0, & \gamma = 0. \end{cases} \tag{B 5b}$$

Thus, by imposing either set of boundary conditions above, we automatically satisfy the global mass conservation constraint. Note that for injection ($\gamma \neq 0$) at the origin ($x = 0$) we need $\left(x^q h^s h_x\right)\big|_{x\to 0}$ to be finite, which is only the case if $h^s h_x = O(1/x^q)$ as $x \to 0$, i.e., the profile and/or its slope blows up at $x = 0$. Clearly, in this case, the lubrication approximation of 1D flow near the origin is violated locally, however, this does not have a significant effect on the gravity current away from this localized region (Huppert 1982; Golding *et al.* 2013). Alternatively, we could solve the PDE on a domain (ℓ, L), where $\ell \approx 0$, enforcing the flux condition $\left(x^q h^s h_x\right)\big|_{x=\ell} = -\frac{\gamma B}{A} t^{\gamma-1} \Rightarrow \left(h^s h_x\right)\big|_{x=\ell} = -\frac{\gamma B}{A\ell^q} t^{\gamma-1}$.

B.2. *Construction of a second-order-accurate scheme with internal iterations*

Now, we introduce the grid-function $h_i^n \approx h(x_i, t^n)$ on the staggered grid $x_i = (i - \frac{1}{2})\Delta x$, where $\Delta x = L/N$. This means that the point $i = 0$ is a half-spacing to the left of $x = 0$, and the point $i = N + 1$ is a half-spacing to the right of $x = L$; thus, $N + 2$ is the total number of spatial grid points. Furthermore, we use the notation

$$\mathcal{L}\,h \equiv \frac{A}{x^p}\frac{\partial}{\partial x}\left(x^q h^s \frac{\partial h}{\partial x}\right), \tag{B 6}$$

and $\mathcal{L}_d$ denotes the discretized counterpart to $\mathcal{L}$, as defined below. We would like to construct a Crank–Nicolson scheme (Crank & Nicolson 1947; Strikwerda 2004) for equation (B 1) via the time discretization

$$\frac{h_i^{n+1} - h_i^n}{\Delta t} = \frac{1}{2}\left(\mathcal{L}_d\, h_i^{n+1} + \mathcal{L}_d\, h_i^n\right), \tag{B 7}$$

which is second-order accurate in time. Now, a second-order central difference approximation to $\mathcal{L}$ can be constructed by treating the "non-Cartesian part" ($p, q \neq 0$) via a weighted difference as in (Christov & Homsy 2009):

$$\mathcal{L}\,h \approx \mathcal{L}_d\,h_i^n = \frac{A}{x_i^p}\left[\frac{x_{i+1/2}^q \psi_{i+1/2}^{n+1/2}\dfrac{(h_{i+1}^n - h_i^n)}{\Delta x} - x_{i-1/2}^q \psi_{i-1/2}^{n+1/2}\dfrac{(h_i^n - h_{i-1}^n)}{\Delta x}}{\Delta x}\right], \quad \text{(B 8)}$$

where we introduced an intermediate variable ψ to denote the grid function of the nonlinear term h^s. To have a nonlinear conservative extension of the Crank–Nicolson scheme for equation (B 1), this term has to be evaluated at the half-time step and on a staggered mesh with respect to x_i (Christov & Deng 2002), i.e.,

$$\psi_{i+1/2}^{n+1/2} \equiv \frac{1}{2}\left\{\frac{1}{2}\left[(h_{i+1}^{n+1})^s + (h_i^{n+1})^s\right] + \frac{1}{2}\left[(h_{i+1}^n)^s + (h_i^n)^s\right]\right\}. \quad \text{(B 9)}$$

Note that if $p = q = s = 0$, then equation (B 8) reduces to the standard three-point second-order central difference formula, namely $\partial^2 h/\partial x^2 \approx (h_{i+1}^n - 2h_i^n + h_{i-1}^n)/(\Delta x)^2$.

With equation (B 8) and equation (B 9) in mind, we shall iteratively find the grid function h_i^{n+1} at the new time stage by replacing it in equation (B 7) with $h_i^{n,k+1}$, where $h_i^{n,0} \equiv h_i^n$ (Yanenko 1971). Thus, the scheme becomes

$$\begin{aligned}\frac{h_i^{n,k+1} - h_i^n}{\Delta t} = {} & \frac{A}{2(\Delta x)^2}\left[\frac{x_{i+1/2}^q}{x_i^p}\psi_{i+1/2}^{n,k+1/2}(h_{i+1}^{n,k+1} - h_i^{n,k+1}) \right.\\ & \left. - \frac{x_{i-1/2}^q}{x_i^p}\psi_{i-1/2}^{n,k+1/2}(h_i^{n,k+1} - h_{i-1}^{n,k+1})\right]\\ & + \frac{A}{2(\Delta x)^2}\left[\frac{x_{i+1/2}^q}{x_i^p}\psi_{i+1/2}^{n,k+1/2}(h_{i+1}^n - h_i^n) - \frac{x_{i-1/2}^q}{x_i^p}\psi_{i-1/2}^{n,k+1/2}(h_i^n - h_{i-1}^n)\right], \quad \text{(B 10)}\end{aligned}$$

which can be rewritten as

$$\begin{aligned}&\left[-\frac{A\Delta t}{2(\Delta x)^2}\frac{x_{i-1/2}^q}{x_i^p}\psi_{i-1/2}^{n,k+1/2}\right]h_{i-1}^{n,k+1}\\ &\quad + \left[1 + \frac{A\Delta t}{2(\Delta x)^2}\left(\frac{x_{i+1/2}^q}{x_i^p}\psi_{i+1/2}^{n,k+1/2} + \frac{x_{i-1/2}^q}{x_i^p}\psi_{i-1/2}^{n,k+1/2}\right)\right]h_i^{n,k+1}\\ &\quad + \left[-\frac{A\Delta t}{2(\Delta x)^2}\frac{x_{i+1/2}^q}{x_i^p}\psi_{i+1/2}^{n,k+1/2}\right]h_{i+1}^{n,k+1}\\ &= h_i^n + \frac{A\Delta t}{2(\Delta x)^2}\left[\frac{x_{i+1/2}^q}{x_i^p}\psi_{i+1/2}^{n,k+1/2}(h_{i+1}^n - h_i^n) - \frac{x_{i-1/2}^q}{x_i^p}\psi_{i-1/2}^{n,k+1/2}(h_i^n - h_{i-1}^n)\right]. \quad \text{(B 11)}\end{aligned}$$

It should be clear that each internal iteration involves the inversion of a tridiagonal matrix, and the scheme has truncation error $O\left[(\Delta x)^2 + (\Delta t)^2\right]$. This is in contrast to the scheme of Diez *et al.* (1992), which has truncation error $O\left[(\Delta x)^2 + (\Delta t)\right]$, is valid only for $p = q$ and requires a "precursor" film ahead of the gravity current.

We construct the boundary conditions semi-implicitly, i.e., we do not take the half time step values of the nonlinear h^s terms but rather the values at the previous time step, so that we can explicitly solve for the h values at the upcoming time step. Thus,

the BCs in equation (B 4) become

$$\frac{1}{2}\left[(h_0^{n,k})^s + (h_1^{n,k})^s\right]\frac{1}{\Delta x}\left(h_1^{n,k+1} - h_0^{n,k+1}\right) = \begin{cases} -\dfrac{\gamma B}{A}t^{\gamma-1}, & \gamma \neq 0, \\ 0, & \gamma = 0, \end{cases} \tag{B 12a}$$

$$\frac{1}{\Delta x}\left(h_{N+1}^{n,k+1} - h_N^{n,k+1}\right) = 0, \tag{B 12b}$$

which can be rewritten as

$$h_0^{n,k+1} - h_1^{n,k+1} = \begin{cases} -\dfrac{2\gamma B t^{\gamma-1}\Delta x}{A[(h_0^{n,k})^s + (h_1^{n,k})^s]}, & \gamma \neq 0, \\ 0, & \gamma = 0, \end{cases} \tag{B 13a}$$

$$-h_N^{n,k+1} + h_{N+1}^{n,k+1} = 0. \tag{B 13b}$$

To perform the internal iterations over k at each time step n, we initialize with $h^{n,0} = h^n$ and continue until K such that $\max_i \left|h_i^{n,K} - h_i^{n,K-1}\right| < 10^{-8}\max_i \left|h_i^{n,K-1}\right|$. For the simulations in the present work, we observe that only a few internal iterations are required to meet the convergence criterion. Then, we set $h^{n+1} = h^{n,K}$ to complete an iteration of the nonlinear conservative Crank–Nicolson scheme.

In a typical simulation used for generating the results in §3, where $s = 1$, we used the initial condition

$$h(x,0) = \begin{cases} 0, & 0 \leqslant x \leqslant 0.8L, \\ 0.1(x - 0.8L), & 0.8L < x \leqslant L. \end{cases} \tag{B 14}$$

This corresponds to $x_f(0)/L = x_0/L = 0.8$, which is comparable to the experiments, and $h(L,0)/L = 0.02 \ll 1$ as required by the lubrication approximation. The value of L is set by the value of A. It should be noted that the shape of the initial condition is "forgotten" in self-similar regime.

B.3. *Convergence of the scheme and conservation properties*

We have verified the second-order of accuracy of the scheme constructed above by comparing the numerical solution to the Barenblatt–Pattle exact point-source solution (Barenblatt 1952; Pattle 1959) on the domain $x \in (-L, L)$ for the axisymmetric case in N dimensions, i.e., $p = q = N - 1$, and s a positive integer. By halving Δt and Δx simultaneously, we observe second-order accuracy of the numerical solution in the L^1 and L^2 norms. Similarly, for both the Barenblatt–Pattle solution on $x \in (-L, L)$ and the problems on $x \in (0, L)$ with the nonlinear boundary conditions above, we have verified that $\int_0^L x^p h \,\mathrm{d}x = Bt^\gamma$ up to numerical precision for all t in each simulation.

REFERENCES

Anderson, D. M., McLaughlin, R. M. & Miller, C. T. 2003 The averaging of gravity currents in porous media. *Phys. Fluids* **15**, 2810–2829.

Angenent, S. B. & Aronson, D. G. 1995 Intermediate asymptotics for convergent viscous gravity currents. *Phys. Fluids* **7**, 223–225.

Barenblatt, G. I. 1952 On some unsteady fluid and gas motions in a porous medium (in Russian). *Prikl. Mat. Mekh. (PMM)* **16**, 67–78.

Barenblatt, G. I. 1996 *Similarity, Self-Similarity, and Intermediate Asymptotics*. Cambridge University Press.

Barenblatt, G. I. & Zel'dovich, Ya. B. 1972 Self-similar solutions as intermediate asymptotics. *Annu. Rev. Fluid Mech.* **4**, 285–312.

Bear, J. 1972 *Dynamics of Fluids in Porous Media*. Elsevier.

Christov, C. I. & Deng, K. 2002 Numerical investigation of quenching for a nonlinear diffusion equation with a singular Neumann boundary condition. *Numer. Methods Partial Differential Eq.* **18**, 429–440.

Christov, C. I. & Homsy, G. M. 2009 Enhancement of transport from drops by steady and modulated electric fields. *Phys. Fluids* **21**, 083102.

Ciriello, V., Di Federico, V., Archetti, R. & Longo, S. 2013 Effect of variable permeability on the propagation of thin gravity currents in porous media. *Int. J. Non-linear Mech.* **57**, 168–175.

Class, H., Ebigbo, A., Helmig, R., Dahle, H. K., Nordbotten, J. M., Celia, M. A., Audigane, P., Darcis, M., Ennis-King, J., Fan, Y., Flemisch, B., Gasda, S. E., Jin, M., Krug, S., Labregere, D., Naderi Beni, A., Pawar, R. J., Sbai, A., Thomas, S. G., Trenty, L. & Wei, L. 2009 A benchmark study on problems related to CO_2 storage in geologic formations. *Comput. Geosci.* **13**, 409–434.

Courant, R. & Friedrichs, K. O. 1999 *Supersonic Flow and Shock Waves*, *Applied Mathematical Sciences*, vol. 21. Springer-Verlag, corrected 5th printing.

Crank, J. & Nicolson, P. 1947 A practical method for numerical evaluation of solutions of partial differential equations of the heat-conduction type. *Proc. Camb. Phil. Soc.* **43**, 50–67.

De Loubens, R. & Ramakrishnan, T. S. 2011 Analysis and computation of gravity-induced migration in porous media. *J. Fluid Mech.* **675**, 60–86.

Detournay, E. 2004 Propagation regimes of fluid-driven fractures in impermeable rocks. *Int. J. Geomech.* **4**, 35–45.

Didden, N. & Maxworthy, T. 1982 Viscous spreading of plane and axisymmetric gravity waves. *J. Fluid Mech.* **121**, 27–42.

Diez, J. A., Gratton, R. & Gratton, J. 1992 Self-similar solution of the second kind for a convergent viscous gravity current. *Phys. Fluids A* **6**, 1148–1155.

Diez, J. A., Thomas, L. P., Betelú, S., Gratton, R., Marino, B., Gratton, J., Aronson, D. G. & Angenent, S. B. 1998 Noncircular converging flows in viscous gravity currents. *Phys. Rev. E* **58**, 6182–6187.

Dullien, F. A. L. 1992 *Porous Media: Fluid Transport and Pore Structure*. Academic Press.

Eggers, J. & Fontelos, M. A 2009 The role of self-similarity in singularities of partial differential equations. *Nonlinearity* **22**, R1–R44.

Flitton, J. C. & King, J. R. 2004 Moving-boundary and fixed-domain problems for a sixth-order thin-film equation. *Eur. J. Appl. Math.* **15**, 713–754.

Golding, M. J., Huppert, H. E. & Neufeld, J. A. 2013 The effects of capillary forces on the axisymmetric propagation of two-phase, constant-flux gravity currents in porous media. *Phys. Fluids* **25**, 036602.

Gratton, J., Mahajan, S. M. & Minotti, F. 1999 Theory of creeping gravity currents of a non-Newtonian liquid. *Phys. Rev. E* **60**, 6090–6097.

Gratton, J. & Minotti, F. 1990 Self-similar viscous gravity currents: phase plane formalism. *J. Fluid Mech.* **210**, 155–182.

Hallez, Y. & Magnaudet, J. 2009 A numerical investigation of horizontal viscous gravity currents. *J. Fluid Mech.* **630**, 71–91.

Hesse, M. A., Tchelepi, H. A., Cantwell, B. J. & Orr Jr, F. M. 2007 Gravity currents in horizontal porous layers: transition from early to late self-similarity. *J. Fluid Mech.* **577**, 363–383.

Homsy, G. M. 1987 Viscous fingering in porous media. *Annu. Rev. Fluid Mech.* **19**, 271–311.

Hoult, D. P. 1972 Oil spreading on the sea. *Annu. Rev. Fluid Mech.* **4**, 341–368.

Huppert, H. E. 1982 The propagation of two-dimensional and axisymmetric viscous gravity currents over a rigid horizontal surface. *J. Fluid Mech.* **121**, 43–58.

Huppert, H. E. 2000 Geological fluid mechanics. In *Perspectives in Fluid Dynamics* (ed. G. K. Batchelor, H. K. Moffatt & M. G. Worster), pp. 447–506. Cambridge University Press.

Huppert, H. E. 2006 Gravity currents: a personal perspective. *J. Fluid Mech.* **554**, 299–322.

Huppert, H. E., Neufeld, J. A. & Strandkvist, C. 2013 The competition between gravity and flow focusing in two-layered porous media. *J. Fluid Mech.* **720**, 5–14.

Huppert, H. E. & Woods, A. W. 1995 Gravity driven flows in porous layers. *J. Fluid Mech.* **292**, 55–69.

King, J. R. & Bowen, M. 2001 Moving boundary problems and non-uniqueness for the thin film equation. *Eur. J. Appl. Math.* **12**, 321–356.

Kochina, I. N., Mikhailov, N. N. & Filinov, M. V. 1983 Groundwater mound damping. *Int. J. Eng. Sci.* **21**, 413–421.

Lister, J. R. 1992 Viscous flows down an inclined plane from point and line sources. *J. Fluid Mech.* **242**, 631–653.

Lyle, S., Huppert, H. E., Hallworth, M., Bickle, M. & Chadwick, A. 2005 Axisymmetric gravity currents in a porous medium. *J. Fluid Mech.* **543**, 293–302.

Monteiro, P. J. M., Rycroft, C. H. & Barenblatt, G. I. 2012 A mathematical model of fluid and gas flow in nanoporous media. *Proc. Natl Acad. Sci. USA* **109**, 20309–20313.

Nordbotten, J. M. & Celia, M. A. 2006 Similarity solutions for fluid injection into confined aquifers. *J. Fluid Mech.* **561**, 307–327.

Parker, T. S. & Chua, L. O. 1989 *Practical Numerical Algorithms for Chaotic Systems*. Springer-Verlag.

Pattle, R. E. 1959 Diffusion from an instantaneous point source with a concentration-dependent coefficient. *Quart. J. Mech. Appl. Math.* **12**, 407–409.

Philip, J. R. 1970 Flow in porous media. *Annu. Rev. Fluid Mech.* **2**, 177–204.

Phillips, O. M. 1991 *Flow and Reactions in Permeable Rocks*. Cambridge University Press.

Pritchard, D. 2007 Gravity currents over fractured substrates in a porous medium. *J. Fluid Mech.* **584**, 415–431.

Saffman, P. G. & Taylor, G. 1958 The penetration of a fluid into a porous medium or Hele-Shaw cell containing a more viscous liquid. *Proc. R. Soc. Lond. A* **245**, 312–329.

Sedov, L. I. 1993 *Similarity and Dimensional Methods in Mechanics*, 10th edn. CRC Press.

Simpson, J. E. 1982 Gravity currents in the laboratory, atmosphere, and ocean. *Annu. Rev. Fluid Mech.* **14**, 213–234.

Spence, D. A. & Sharp, P. 1985 Self-similar solutions for elastohydrodynamic cavity flow. *Proc. R. Soc. Lond. A* **400**, 289–313.

Strikwerda, J. 2004 *Finite Difference Schemes and Partial Differential Equations*. Society for Industrial and Applied Mathematics.

Takagi, D. & Huppert, H. E. 2007 The effect of confining boundaries on viscous gravity currents. *J. Fluid Mech.* **577**, 495–505.

Vella, D. & Huppert, H. E. 2006 Gravity currents in a porous medium at an inclined plane. *J. Fluid Mech.* **555**, 353–362.

Witelski, T. P. 1998 Horizontal infiltration into wet soil. *Water Res. Res.* **30**, 1859–1863.

Woods, A. W. & Farcas, A. 2009 Capillary entry pressure and the leakage of gravity currents through a sloping layered permeable rock. *J. Fluid Mech.* **618**, 361–379.

Yanenko, N. N. 1971 *The Method of Fractional Steps*. Springer-Verlag, english translation edited by M. Hoult.

Zheng, Z., Larson, E. D., Li, Z., Liu, G. & Williams, R. H. 2010 Near-term mega-scale CO_2 capture and storage demonstration opportunities in China. *Energy Environ. Sci.* **3**, 1153–1169.

Zheng, Z., Soh, B., Huppert, H. E. & Stone, H. A. 2013 Fluid drainage from the edge of a porous reservoir. *J. Fluid Mech.* **718**, 558–568.